Morphology of Neutralized Low Molecular Weight Maleated Ethylene−Propylene Copolymers (MAn-*g*-EPM) As Investigated by Small-Angle X-ray Scattering

M. E. L. Wouters,† J. G. P. Goossens,* and F. L. Binsbergen

Eindhoven Polymer Laboratories, Department of Chemical Engineering, Eindhoven University of Technology, P.O. Box 513, 5600 MB Eindhoven, The Netherlands

Received April 26, 2001; Revised Manuscript Received October 2, 2001

ABSTRACT: The thermoreversible nature of the ionic associations in aggregates makes ionomers with a low glass transition temperature interesting candidates for thermoplastic elastomers. In this paper, a low-T_g ionomer based on low molecular weight ethylene−propylene copolymers modified by maleic anhydride (MAn-*g*-EPM) is introduced, and the morphology of a series of ionomers, neutralized with Cs^+, Na^+, K^+, Li^+, Zn^{2+}, Ba^{2+}, and Mg^{2+}, was investigated with small-angle X-ray scattering (SAXS). To determine the size and composition of the ionic aggregates, the observed SAXS peak was interpreted with the help of the Yarusso−Cooper model, which describes the ionomer morphology by spherical aggregates of the ionic species with a high electron density surrounded by a layer with a restricted mobility. The results from the ionomer precursors suggest that there is a critical concentration above which aggregation of the polar groups in the apolar matrix occurs. Upon increasing degree of neutralization, the average dimension of the aggregate remains almost constant, while the restricted mobility layer increases. The size of the aggregates is much larger in comparison to other ionomer systems, and as a consequence, the number of acid groups within an aggregate is much larger. For low degrees of neutralization, it was shown that the aggregates contain a large fraction of EPM fragments of at least 60 vol %. For the ionomers neutralized with divalent cations, it was observed that the morphology changes drastically beyond degrees of neutralization of 50%; the number of the aggregates decreases, and the size increases. This was explained with the help of the coordination mechanism.

Introduction

Ionomers are ion-containing polymers consisting of hydrophobic backbones with a relatively small fraction of monomer units having an ionic functionality either as pendant group or incorporated in the main chain. Mostly carboxylic, sulfonic, and phosphoric acids are used, which are partially or fully neutralized with metal cations. Although many types of ionomers have been developed to date, Surlyn and Nafion are the most well-known commercialized ionomers.

A large number of papers have appeared on the microstructure of ionomers and showed that the ionic groups tend to form microphase-separated ionic aggregates with sizes in the order of nanometers, dispersed in the hydrophobic polymer matrix due to the large difference in dielectric constant. These ionic aggregates are often called multiplets, ionic clusters, or ionic domains and are responsible for the unique physicochemical properties of ionomers, since they can behave as thermoreversible cross-links or reinforcing fillers.[1−4]

The thermoreversible nature of the ionic associations in the aggregates makes ionomers with a low T_g interesting candidates for thermoplastic elastomers, which are polymers that behave like cross-linked elastomers at service temperature but can be melt processed at elevated temperatures. An example of such a low-T_g noncrystalline ionomer is poly(ethylene-*co*-methacrylic acid) (EMAA) with high MAA contents.[5] By using high amounts of MAA, the crystallinity can be suppressed, but the melt viscosity is also affected. Another example is sulfonated EPDM, a terpolymer of ethylene, propylene, and a diene monomer.[6−9] A substantial improvement in mechanical properties, such as tensile modulus and strength, could be obtained by the introduction of small amounts of zinc sulfonate groups, obtained by sulfonating the EPDM with acetyl sulfate and neutralization by zinc acetate.

Though at higher temperatures weakening of the ionic interactions occurred, the ionic interactions were too strong and resulted in very high melt viscosities at conventional processing temperatures. The processability of these systems could be enhanced by adding polar plasticizers, which selectively plasticize the ionic aggregates.[10,11] This reduces the melt viscosity substantially but also deteriorates the mechanical properties.

In the study of Lundberg and Makowski,[12] it was shown that sulfonated ionomers associate stronger than analogous carboxylated systems. The melt viscosities of the used sulfonated ionomers are about 2−3 orders of magnitude higher than the carboxylated analogues at a given level of functionality and temperature. Therefore, the use of a *carboxylated elastomer* is preferred. Additionally, sulfonated elastomers require complete neutralization because of the corrosivity of the free sulfonic acid groups in partially neutralized ionomers. For carboxylated elastomers *partial neutralization* is allowed; the degree of neutralization can therefore be used as an additional variable to control the properties of the ionomer. In this paper a low-T_g ionomer based on an ethylene−propylene copolymer (EPM) will be introduced which is prepared by modification of EPM with maleic anhydride (MAn). When using a maleated

† Present address: TNO Industrial Technology, Division of Materials Technology, P.O. Box 6235, 5600 HE Eindhoven, The Netherlands.

* Corresponding author.

10.1021/ma0107253 CCC: $22.00
Published on Web 12/04/2001

ethylene−propylene copolymer (MAn-*g*-EPM) as ionomer precursor, an ionomer based on a carboxylic acid functionality is obtained. Moreover, MAn is a suitable monomer to graft onto an EPM because it has a low tendency to homopolymerize, resulting in well-defined grafts.

As for all ionomers given the microphase-separated structures, the mechanical properties and rheology of the MAn-*g*-EPM-based ionomers are highly dependent on the morphology. The morphology of random ionomers and the structure of the ionic aggregates have been extensively studied, primarily using small-angle X-ray scattering (SAXS). The SAXS profile has a characteristic feature, the so-called *ionic peak*. For most reported systems, this peak is usually observed at $q = 0.1-0.4$ Å^{-1} ($q = (4\pi/\lambda) \sin \theta$, where λ is the X-ray wavelength and 2θ is the scattering angle). In some cases, also a strong upturn in scattered intensity is observed near $q = 0$. Several structural models have been proposed to explain both the ionic peak and the upturn. To explain the ionic peak, all proposed models assume ionic aggregates with dimensions of 10−100 Å as the basic scattering entity, but the scattering models are divided into two categories: *interparticle* interference models and *intraparticle* interference models. Since both models can produce a single broad peak, it has been very difficult to make a distinction between those models. For the interparticle models, a subdivision can be made between models which are based on considering the ionic domains as scattering entities placed on a paracrystalline lattice[13] and models that consider the ionic domains as scattering entities with a liquidlike order.[14−16] The most important model of this class was proposed by Yarusso and Cooper.[14] They used a modified hard-sphere model in which the ionic domains have a liquidlike order and a distance of closest approach determined by a layer of hydrocarbon chains with a restricted mobility attached to and surrounding each ionic domain. The model was in excellent agreement with the experimentally determined ionic peak of various sulfonated polystyrene systems.[14] The restricted mobility close to the ionic domain was one of the features which lead Eisenberg, Hird, and Moore to propose a new model.[17] It is a revision of the original model from Eisenberg with the addition of introducing a critical ion content above which the regions of restricted mobility start to overlap and form domains large enough to exhibit a separate glass transition temperature (T_g). The core−shell model as proposed by MacKnight et al.[18] is an example of an intraparticle interference model. In this model, it is assumed that the ion pairs form a core that is surrounded by a shell of material of low electron density, which, in turn, is surrounded by another shell of material with a somewhat higher electron density (but lower than the core itself).

It is therefore evident that the interpretation of the observed *ionic peak* in terms of size and eventually the composition of the ionic aggregates depends on the morphological model used to fit the experimental data. Several of the models discussed above were evaluated and the fits were compared with experimental data.[19] The Yarusso and Cooper (Y−C) liquidlike model[14] proved to be the best model to interpret the experimental SAXS data. This choice is also supported by the structure of the ionomer precursors, which also showed a peak in the SAXS pattern similar to the sulfonated polystyrene systems used by Yarusso and Cooper. One essential feature of the Y−C model is the presence of a layer of matrix material with a restricted mobility. Solid-state NMR results of the MAn-*g*-EPM-based ionomers showed that there are indeed two populations of EPM molecules with different mobilities—a further motivation for the Y−C model irrespective of the SAXS data.[20]

In this paper, SAXS results of MAn-*g*-EPM-based ionomers will be presented, and the morphology will be discussed with the help of the Yarusso−Cooper model. Because of the large difference in dielectric constant between maleic anhydride and the EPM copolymer, it may be expected that microphase separation can occur in the ionomer precursors. Therefore, the structure of EPM copolymers with a constant molecular weight has been studied as a function of the degree of grafting, i.e., number of functional groups. The effects of degree of neutralization and choice of counterion on the morphology have been studied using MAn-*g*-EPMs with constant molecular weight and degree of grafting. The interpretation of the observed *ionic peak* allows the determination of the size and eventually the composition of the ionic aggregates which is important for the mechanical properties.[19]

Experimental Section

Preparation of Ionomer Precursor. In a double-walled glass reactor equipped with a nitrogen inlet, septum, and helical impeller, the copolymer (45 wt % ethylene, 55 wt % propylene, $M_n = 11$ kg mol^{-1}) was dissolved in xylene (a mixture of xylene isomers (*o*-, *m*-, and *p*-xylene, supplied by Aldrich) at the reaction temperature (130 °C). When dissolution of the polymer was completed, maleic anhydride (MAn, Merck, >99%) was added to the solution. After all maleic anhydride was dissolved, *tert*-butylperoxy benzoate (Trigonox C, Akzo Nobel) was added via the septum. After a reaction time of at least 5 half-life times of the peroxide, the mixture was poured into acetone (using 1 L of acetone for a 150 mL reaction mixture) under vigorous stirring to remove unreacted maleic anhydride. The precipitate was washed at least three times with smaller portions of acetone (150 mL aliquots) to ensure that all traces of unreacted maleic anhydride and peroxide were removed. The product was dried overnight in a vacuum oven at 80 °C with a nitrogen flush. The amount of grafted maleic anhydride was determined by potentiometric titration (see next section).

Potentiometric Titration. The amount of grafted maleic anhydride was determined by potentiometric titration as follows: the maleated product was dried at 150 °C for 1 h under vacuum and nitrogen flush to close hydrolyzed anhydride rings. Subsequently, a sample of the dried product was dissolved in a toluene/2-propanol mixture (9/1 v/v). A 0.03 N solution of tetrabutylammonium hydroxide in 2-propanol was used as titrant. The potentiometric titration was performed by a Methrom E670 Titroprocessor. The degree of grafting (DG) can be calculated by eq 1.

$$\mathrm{DG} = \frac{V_{\mathrm{titrant}} N M_{\mathrm{MAn}} \times 100 \times 100}{C_{\mathrm{pol}} m_{\mathrm{sol}} \times 1000} \tag{1}$$

where V_{titrant} = volume of titrant required for titration of the polymer solution (mL), N = normality of the TBAOH−solution (mol L^{-1}), M_{MAn} = molar mass of grafted maleic anhydride (98.06 g mol^{-1}), C_{pol} = concentration of the polymer solution (wt %), and m_{sol} = mass of the polymer solution that is titrated (g). A practical unit to express the acid content for random ionomers is equivalent acid per unit weight of polymer (χ). For example, the Surlyn materials have an acid content of approximately 1 equiv kg^{-1}. Conversion of the degree of grafting in weight percentage to equivalent acid per unit of weight for the MAn-*g*-EPM ionomer precursor is described by eq 2.

Maleic anhydride (MAn) is converted to carboxylic acid by the addition of water; upon hydrolysis 2 mol of carboxylic acid is formed from 1 mol of anhydride.

$$\chi = \frac{\mathrm{DG}}{100\%} \frac{1000}{M_{\mathrm{MAn}}} 2 \qquad (2)$$

Neutralization Procedure. The modified ethylene−propylene copolymer (MAn-*g*-EPM) was dried for 18 h at 100 °C under a nitrogen atmosphere before neutralization. Typically, 15 g of MAn-*g*-EPM was dissolved in a mixture of 135 g of toluene and 15 g of 2-propanol at 80 °C. After complete dissolution, 10 g of an aqueous solution containing the required amount of base, e.g., zinc acetate dihydrate ($ZnC_4H_6O_4 \cdot 2H_2O$ (ZnAc), Fluka, p.a. 99.5%), was added. The two-phase reaction mixture was mixed for 15 min. Then, approximately 75 g of solvent was distilled off, and new solvent (toluene/2-propanol) was added to the viscous system to remove the excess of water. The mixture was allowed to homogenize at 80 °C for 30 min, after which the polymer was evaporated to dryness and dried under vacuum at 100 °C for 16 h. The degree of neutralization (DN) can be calculated as follows:

$$\mathrm{DN} = \frac{\nu m_{\mathrm{ZnAc}} \times 1000}{M_{\mathrm{ZnAc}} \chi m_{\mathrm{product}}} \times 100\% \qquad (3)$$

where ν = valency of the metal ion (in the case of zinc ν equals 2), m_{ZnAc} = mass of zinc-acetate dihydrate added (g), M_{ZnAc} = molecular weight of zinc acetate dihydrate (219.50 g mol^{-1}), and m_{product} = mass of MAn-*g*-EPM used (g).

SAXS. SAXS data were collected at beamline 8.2 of the Synchrotron Radiation Source (SRS) at the CLRC Daresbury Laboratory, Warrington, U.K. A detailed description of the experimental setup is given elsewhere.[21] The SAXS profiles were collected with a quadrant detector, calibrated with silver behenate.[22] A parallel ionization detector was placed in front and after the sample, to record the incident and transmitted intensity. The detector was positioned at 1.5 m distance from the sample. All samples were measured for 60 s. The data of the SAXS experiments are presented as the normalized intensity per unit sample volume as a function of q ($I(q)\{I_e(q)V\}^{-1}$). For this purpose, the obtained experimental data were corrected for background scattering, detector response, and sample thickness (transmittance). The resulting curves were converted to absolute scattering power by comparison with the scattering from a Lupolen standard, measured, and corrected by the same procedure as the ionomer samples.[23]

Thin films of the ionomers were pressed between poly(tetrafluoroethylene) sheets at 150 °C in a press. The films were pressed in cardboard sample holders to obtain a uniform sample thickness of 0.33 mm. Water absorption by the ionomers during storage was prevented by placing the freshly prepared samples in sealed sample containers, which contained silica gel.

Motivation for the Use of the Yarusso−Cooper Model. There are two types of models that attribute the ionomer SAXS peak to interparticle interference and that are able to calculate the SAXS profile. These two models are the paracrystalline lattice model[13] and the liquidlike interference model.[14−16]

The paracrystalline lattice model is not suitable for the ionomer systems studied. The shape of the theoretical SAXS peak is not correct; the peak in the experimental scattering profile is not as sharp as the theoretical peak. The actual order that exists can be modeled more accurately with the approach of the liquidlike ordering. Of the existing liquidlike interference models discussed in the literature, the morphological concept described by the Yarusso−Cooper model fitted very well to the experimental SAXS profiles. Moreover, the trends observed by Yarusso and Cooper for molecular weight or ion content variation correspond to our data.[19]

To further justify the choice of the Yarusso−Cooper model, solid-state nuclear magnetic resonance (NMR) was used. The relaxation experiments showed that MAn, its salts with Zn^{2+}, and a fraction of EPM chain fragments form rigid aggregates. Three different types of protons were detected in the ionomers and ionomer precursor, which can be attributed to low mobile protons inside the ionic aggregates, protons of EPM network chains, and protons of network imperfections such as dangling ends.[20]

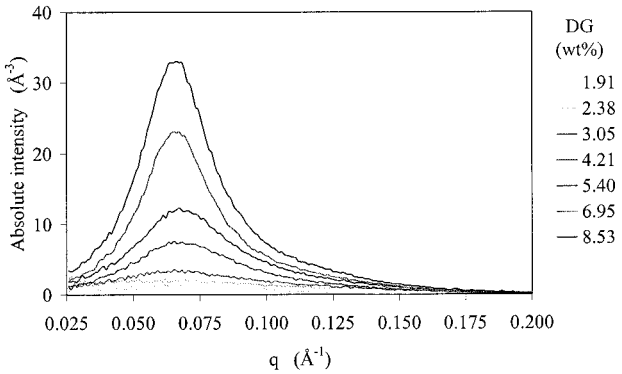

Figure 1. SAXS profiles of MAn-*g*-EPM ionomer precursors with a variation in degree of grafting (DG).

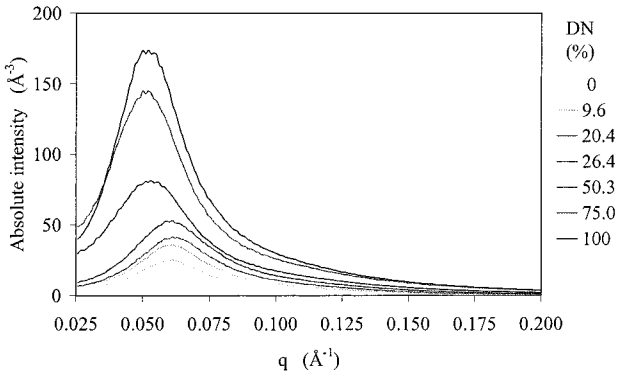

Figure 2. SAXS profiles for zinc ionomers based on MAn-*g*-EPM (DG = 7.33 wt %) with various degrees of neutralization (DN).

Results

To obtain a complete picture of the ionomer morphology, the effect of ionomer composition on the morphology was studied with SAXS. All ionomers were prepared from MAn-*g*-EPM and the effect of the degree of grafting, degree of neutralization, and type of cation was studied, and the results will be presented in this section.

Effect of Degree of Grafting (MAn Concentration) in Ionomer Precursors. A range of ionomer precursors with a variation in degree of grafted maleic anhydride was studied. Figure 1 shows the SAXS peak in the ionomer precursor materials as a function of the degree of grafting (DG) varying from 0 (the parent polyolefin) up to 8.53 wt %.

One of the most remarkable observations is the presence of a peak in the scattering profile of the ionomer precursor (MAn-*g*-EPM, DN = 0%). The ionomer precursors with a degree of grafting below approximately 3 wt % grafted MAn units do not exhibit a distinct peak in the SAXS profile. Upon increasing degree of grafting, the intensity of the peak increases, while the position of the peak remains unchanged.

Effect of Degree of Neutralization. The SAXS data obtained from zinc ionomers based on MAn-*g*-EPM with various degrees of neutralization (DN) are shown in Figure 2. As already mentioned, the observed peak in the ionomer precursor SAXS profile implies that the

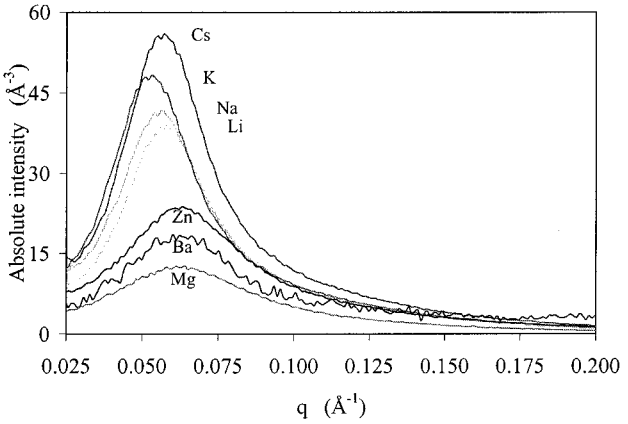

Figure 3. Effect of cation on the SAXS profile of MAn-*g*-EPM-based ionomers (DG = 5.03 wt %) with a degree of neutralization of approximately 50%.

MAn-*g*-EPM already contains aggregates that differ in electron density from the polymer matrix. The intensity of the scattering peak increases upon increasing neutralization. Up to 50% neutralization the intensity of the peak increases while the position of the peak is constant. Besides the increase in intensity of the peak in the SAXS profile, the position of the peak maximum shifts to lower q values when DN = 50% is exceeded. The peak maximum shifts from 0.061 Å^{-1} for DN = 0% to approximately 0.052 Å^{-1} for DN = 100%.

Effect of Nature and Size of the Cation. By using various metal acetates as neutralizing agents, the effect of type of cation, ionic radius, and valency on the ionomer morphology was studied. The alkali metals Li, Na, K, and Cs and the alkaline earth metals Mg and Ba plus Zn were used. The ionic radii (R_{ionic}) of the cations vary from 0.65 to 1.67 Å. These different cations cover a range of valencies (ν) from 1 to 2.

The tendency as observed in the zinc ionomer series (variation of DN) was also observed in the ionomer series using other cations. The intensity of the peak in the SAXS profile increases upon neutralization, and the peak shifts to lower q values. However, at equal degree of neutralization and grafting the different cation types have different SAXS profiles. This is shown in Figure 3 for ionomers with DG = 5.03 wt % neutralized to approximately 50%.

The peak of the alkaline metal cations is positioned at lower angles compared to the peak of the alkaline earth metal cations. The peak position in the SAXS profile of the ionomers changes with type of cation in the following order: Cs < K < Na < Li < Zn ≈ Ba ≈ Mg. Considering the electron density differences between the cations, it can be expected that the absolute intensity of the SAXS peak maximum varies, but the trend is not consistent with the theoretical increment in electron density. Both observations (peak position and intensity) suggest that the structure and composition of the ionic aggregates are different for the different cations.

Discussion

In this section the results of the SAXS experiments are used to elucidate the ionomer morphology. By fitting the earlier discussed Yarusso−Cooper model to the measured SAXS data, the effects of DG, DN, and type of cation on the ionomer morphology will be discussed. The fitting procedure is discussed in Appendix A.

For all recorded SAXS profiles of the ionomers and ionomer precursors, the data were fitted to gain insight in the effect of the various experimental variables on the dimensions (R_1 and R_{CA}) of the scattering particles. The amount of scattering particles can be deduced from the average sample volume per scattering particle (V_p). The number of scattering particles in the sample volume is equal to V_p^{-1}. Assuming that all grafted MAn units are phase separated from the EPM matrix, which is plausible based on the polarity differences, the value of the electron density difference between the scattering particle and the EPM matrix (ρ) can provide information about the composition of the scattering particle.

Effect of Degree of Grafting (MAn Concentration). A range of ionomer precursors with a variation in degree of grafted maleic anhydride (DG) was studied. One of the most remarkable observations is the scattering profile of the ionomer precursor (MAn-*g*-EPM, DN = 0%). As already pointed out in the previous part, the presence of a peak in the ionomer precursor material is at variance with ionomer systems studied based on ethylene−methacrylic acid copolymers (Surlyn). In these systems, the so-called "ionic peak" is only observed after neutralization of the acid groups of the copolymer.[13,24,25] In the case of sulfonated styrene-based ionomers the "ionic peak" is also observed in the ionomer precursor,[14] although there is some inconsistency in the literature.[26]

It was checked whether the peak in the SAXS profile is related to the structure of the ethylene−propylene copolymer (EPM), though the parent polyolefin is assumed to be fully amorphous. The parent EPM showed no additional scattering.

The ionomer precursors having a degree of grafting below approximately 3 wt % grafted MAn did not exhibit a distinct peak in the SAXS profile, suggesting that a critical concentration is required to induce microphase separation. The aggregate formation in the ionomer precursor may be explained by the large difference in polarity between the grafted MAn groups and the EPM matrix. The polarity difference plays an important role in the aggregate formation.[27−29] The major energy gain for aggregation in a hydrocarbon matrix comes from the interaction between the polar groups. This interaction can be dipole−dipole interaction, hydrogen bonding, or specific atom-to-atom coordination. Hydrogen bonding is a strong interaction compared to dipole−dipole interaction. In the MAn-*g*-EPM-based ionomer precursors, the polar groups are anhydride groups and not carboxylic acid groups, unlike in for instance ethylene−methacrylic copolymers. Consequently, mutual hydrogen bonding is absent. The attractive force between the polar groups is dipole−dipole interaction. On the basis of this weaker interaction, large aggregates can be formed and as a result the peak position of the MAn-*g*-EPM-based ionomers differs from the peak position as observed for ethylene−methacrylic copolymer-based systems.

The position of the peak in the SAXS profile of the ionomer precursor does not shift when the degree of grafting increases, as could be seen in Figure 1. The only difference between the profiles of the precursors is the intensity of the scattering peak. Table 1 shows the dimensions of the scattering particles, determined by using the Yarusso−Cooper model to fit the SAXS data. Besides the best fit parameters of the model, the acid content (χ), the volume fraction of grafted MAn (V_{MAn},

Table 1. Best-Fit Parameters of the Yarusso−Cooper Model and Calculated Characteristic Parameters for Ionomer Precursors Based on MAn-*g*-EPM as a Function of DG

DG (wt %)	R_1 (Å)	R_{CA} (Å)	V_p (Å^3)	ρ (e$^-$·Å^{-3})	χ (equiv kg^{-1})	V_{MAn}	$R_{CA} - R_1$ (Å)	V_1 (Å^3)	V_1/V_p	$V_{MAn}/(V_1/V_p)$	Ξ
4.21	20.50	39.98	4.96×10^5	0.053	0.86	0.024	19.48	3.61×10^4	0.073	0.34	112
5.40	20.70	40.40	4.62×10^5	0.061	1.10	0.032	19.70	3.71×10^4	0.080	0.39	134
6.95	22.09	42.49	4.14×10^5	0.059	1.42	0.041	20.40	4.52×10^4	0.109	0.37	154
8.53	22.64	42.59	4.18×10^5	0.067	1.74	0.050	19.95	4.86×10^4	0.116	0.43	191

Table 2. Best-Fit Parameters of the Yarusso−Cooper Model and Calculated Characteristic Parameters for Zinc Ionomers Based on MAn-*g*-EPM with a Variation in Degree of Neutralization (DG = 7.33 wt %, χ = 1.50 equiv kg^{-1}, V_{MAn} = 0.043)

DN (%)	q_{peak} (Å^{-1})	R_1 (Å)	R_{CA} (Å)	V_p (Å^3)	ρ (e$^-$ Å^{-3})	$R_{CA} - R_1$ (Å)	V_1 (Å^3)	V_p^{-1} (Å^{-3})	V_1/V_p	$V_{MAn}/(V_1/V_p)$	Ξ
0	0.061	23.96	46.04	6.18×10^5	0.063	22.08	5.76×10^4	1.62×10^{-6}	0.093	0.46	243
10	0.061	22.64	45.76	6.12×10^5	0.087	23.12	4.86×10^4	1.63×10^{-6}	0.079	0.54	240
20	0.061	21.75	44.94	6.03×10^5	0.106	23.19	4.31×10^4	1.66×10^{-6}	0.071	0.60	237
25	0.061	21.63	45.77	6.71×10^5	0.130	24.14	4.24×10^4	1.49×10^{-6}	0.063	0.68	263
50	0.053	24.78	52.06	1.32×10^6	0.162	27.28	6.37×10^4	7.58×10^{-7}	0.048	0.89	518
75	0.052	25.94	54.04	1.31×10^6	0.184	28.10	7.31×10^4	7.63×10^{-7}	0.056	0.77	514
100	0.052	25.30	53.41	1.06×10^6	0.187	28.11	6.78×10^4	9.43×10^{-7}	0.064	0.67	416

see eq 4), thickness of the restricted mobility layer ($R_{CA} - R_1$), volume fraction of the scattering particle (V_1/V_p), and the number of MAn units per scattering particle (Ξ, see eq 5) are presented in this table.

The value of the volume fraction of grafted MAn was calculated using DG (wt %) and the average densities of EPM (855 kg m^{-3}) and MAn (1500 kg m^{-3}):

$$V_{MAn} = \frac{DG/1500}{\{(100 - DG)/855\} + (DG/1500)} \quad (4)$$

The number of grafted MAn units present in a scattering aggregate (Ξ) was calculated using the acid content (χ), the average density of the MAn-*g*-EPM (875 kg m^{-3}), the Avogadro number (N_{Av}), and the average sample volume in which one aggregate is positioned (V_p):

$$\Xi = \frac{1}{2}\chi(875 \times 10^{-30})N_{Av}V_p \quad (5)$$

Upon increasing degree of grafting the radius R_1 (and thus volume V_1) of the scattering particle increases only slightly, while the volume fraction of aggregates (V_1/V_p) increases more pronounced, as can be expected. The thickness of the restricted mobility layer ($R_1 - R_{CA}$) remains almost constant. From the number of grafted MAn units inside an aggregate (Ξ in Table 1), it is sterically incomprehensible that all polymer segments are excluded from these aggregates. As a consequence, the aggregate is diluted with EPM chain fragments. The volume fraction of MAn in the aggregate can be calculated by the ratio of the volume fraction of MAn in the sample (V_{MAn}) to the volume fraction of aggregates in the sample (V_1/V_p):

$$V_{MAn,aggr} = \frac{V_{MAn}}{V_1/V_p} \quad (6)$$

The volume fraction of EPM in the aggregate is equal to

$$V_{EPM,aggr} = 1 - \frac{V_{MAn}}{V_1/V_p} \quad (7)$$

From Table 1 it can be derived that about 40% of the volume of the scattering aggregate is occupied by the grafted MAn units; the remaining volume is occupied by EPM backbone segments. This lowers the electron density difference between the aggregate and the EPM matrix. The results of the electron density difference ρ supports the assumption that all grafted MAn units are inside the scattering aggregate accompanied by EPM chain fragments, since the estimated value for ρ is in all cases smaller than the maximum value of 0.175 e$^-$ Å^{-3}, which is the electron density difference between MAn and EPM.

Effect of Degree of Neutralization. Figure 2 showed that on increasing degree of neutralization (DN) with Zn as cation the intensity of the peak in the SAXS profile increases and that the peak position starts to shift to lower q values from degree of neutralization of approximately 50% and higher. The SAXS profiles of this series of ionomers were also evaluated using the Yarusso−Cooper model. The results of the evaluation are presented in Table 2. In the region of 0−50% neutralization, R_1 decreases slightly, while R_{CA} remains constant. This may be explained by the tightening of the polar groups as a result of the formation of ionic bonds. At DN = 50%, it can be observed that the values of R_1 and R_{CA} suddenly increase, while the number density of scattering particles ($1/V_p$) shows a sudden drop. This change may be explained by the coordination mechanism of MAn with the zinc cation. Upon neutralization to 50%, it seems that mainly one of the two available acid groups is involved in the coordination with the counterion, which is reasonable considering the different pK_a values of the carboxylic acid groups. The second carboxylic acid group is mainly involved in the coordination of the cation for neutralization levels beyond 50%. Because of the steric arrangement and aggregation of the acid groups, Ξ increases when the degree of neutralization exceeds 50%. More insight in the exact coordination mechanism can, in principle, obtained from for instance infrared or Raman spectroscopy, but no clear distinction could be made.

Upon increasing degree of neutralization, the volume fraction of MAn in the aggregate increases and the number density of particles is decreasing. It is anticipated that the polarity of the aggregate increases and, as a consequence, the packing of the polar groups will be denser as the MAn groups are pulled in the aggregate. Since the size of the aggregate is only slightly increasing, the number density of scattering particles must decrease. The electron density difference between the aggregate and the matrix originates from the grafted MAn and cations present. The electron density of the scattering aggregate is calculated using the known volume fraction of MAn (V_{MAn}), V_p, and V_1 and the electron densities of MAn, its salt, and EPM ($\rho_{MAn-salt}$

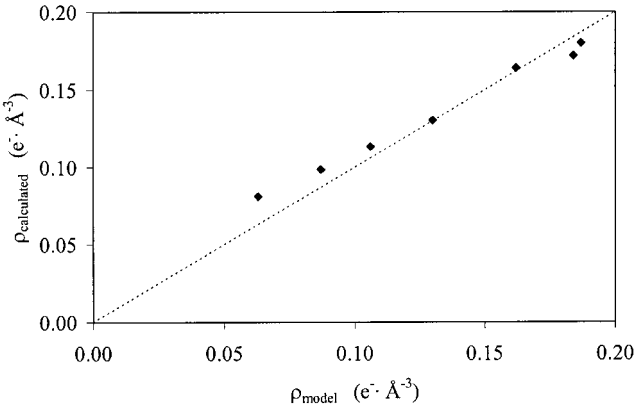

Figure 4. Comparison of the estimated electron density difference using the Yarusso−Cooper model (ρ_{model}) and the calculated electron density difference ($\rho_{calculated}$) as determined from the sample composition.

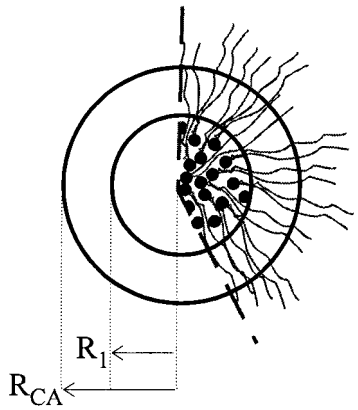

Figure 5. Schematic representation of an aggregate in MAn-*g*-EPM-based ionomer precursors. The black spots represent a grafted MAn unit.

and ρ_{EPM}). Equation 8 can be used to calculate the electron density difference of the aggregate:

$$\rho_{calculated} = \left(\frac{\{V_p V_{MAn}\rho_{MAn-salt}\} + \{(V_1 - (V_p V_{MAn}))\rho_{EPM}\}}{V_1}\right) - \rho_{EPM} \quad (8)$$

$$\rho_{MAn-salt} = \frac{(100 - DN)\rho_{MAn} + DN\rho_{ZnAc_2}}{100} \quad (9)$$

with $\rho_{EPM} = 0.293$ e$^-$ Å^{-3}, $\rho_{MAn} = 0.468$ e$^-$ Å^{-3}, and $\rho_{ZnAc_2} = 0.531$ e$^-$ Å^{-3}.

The comparison of the calculated electron density difference and the fitted value for the electron density difference from the Yarusso−Cooper model as a function of DN is presented in Figure 4. The discrepancy between the calculated and fitted value of ρ at low degrees of neutralization may be found by the fact that the electron density of crystalline zinc acetate dihydrate is used in the calculations, while the anionic packing is less dense.

On the basis of these results and the results from the ionomer precusors, it can be concluded that the ionic aggregates contain, besides the polar groups, EPM chain fragments. In Figure 5 we have tried to give a schematic representation of such an aggregate in MAn-*g*-EPM-based ionomers independent of DN. This schematic representation suggests that the electron density profile of the aggregate is not constant within the spherical aggregate, while in the Y−C model a constant electron density in the scattering particle is assumed. To check the influence of the electron density profile in the aggregate on the fitting results, the Y−C model was modified by using two radius-dependent electron density profiles as depicted in Figure 6b,c. In this way, ρ was made radius dependent and put in eq A to calculate the scattering intensity. In principle, the Φ function should have been adapted as well (see ref 5). For simplicity, we used the aforementioned approach. When the electron density of the scattering particle decreases linearly as a function of the radius of the scattering sphere (Figure 6b), the modeled scattering profile does not change significantly. The values of R_1, R_{CA}, and ρ are slightly larger compared to the model with constant electron density, but even a gradually decreasing electron density profile as depicted in Figure 6c does not improve the fit of the scattered intensity profile, while the total number of electrons per scattering particle remains constant.[19] Therefore, the original model concept as proposed by Yarusso and Cooper[14] was used for the evaluation of the SAXS profiles of the MAn-*g*-EPM-based ionomers because the interpretation of the results of the fitting is easier.

Effect of Nature and Size of the Cation. The effect of the type of counterion, ionic radius, and valency on ionomer morphology was studied using a range of metal acetates for the neutralization of MAn-*g*-EPM (DG = 5.03 wt %). The ionic radii (R_{ionic}) of the cations vary from 0.65 to 1.67 Å and cover different valencies (ν) (summarized in Table 3).

The ionomers were neutralized to different degrees of neutralization. The tendency as observed for zinc ionomers with a constant degree of grafting is similar for the other divalent cations. At equal degree of neutralization and degree of grafting the different cation types result in different SAXS profiles, as shown in Figure 3.

The effect of the counterions on the morphology will be discussed by comparing the results of the 25% neutralized ionomers presented in Table 3. In this table, the best fit parameters of the Y−C model and the calculated thickness of the restricted mobility layer and number of grafted MAn units inside an aggregate (Ξ) are presented. The dependency of aggregate radius on valency may be explained by the coordination mechanism of the grafted maleic anhydride. When monovalent cations are considered, these cations are coordinated by one acid group, and probably, there is no difference in structure when the first or the second acid group of the grafted MAn is neutralized. In the case of divalent cations, which are coordinated by two acid groups, there is a preference for the first acid group to be neutralized. The neutralization mechanism results in tightening of the aggregate beyond 50%, because after all "single" acid groups have been consumed the second acid groups participate in the coordination.

The observed changes in aggregate radius upon increasing cation radius in the case of the alkali metal cation neutralized ionomers differ from the changes observed in the alkali earth metal cation neutralized ionomers. In the case of the alkali metal cations, the aggregate radius of the core (R_1) increases as well as the radius of closest approach (R_{CA}) upon increasing ionic radius. The thickness of the immobilized layer and the number of grafted MAn units inside an aggregate (Ξ) increase also. However, in the alkaline earth metal cation series R_1 and Ξ decrease upon increasing cation

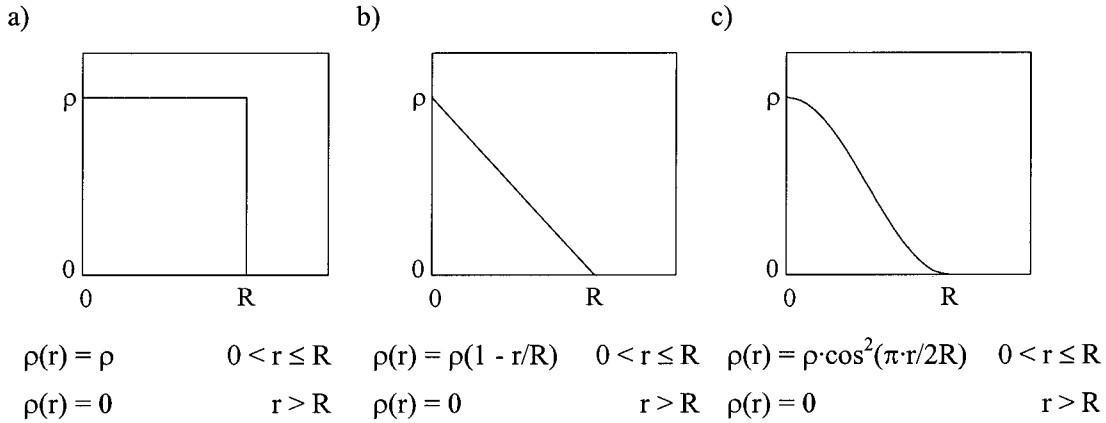

Figure 6. Different electron density profiles used to improve the quality of the fit of theoretical scattering of the Yarusso−Cooper model to the experimental SAXS data.

Table 3. Best-Fit Parameters of the Yarusso−Cooper Model for Ionomers Based on MAn-*g*-EPM with a Variation of Cation (DG = 5.03 wt %, χ = 1.03 equiv kg^{-1}, V_{MAn} = 0.029, DN = 25%)

cation	ν	R_{ionic} (Å)	ν/R_{ionic} (Å^{-1})	R_1 (Å)	R_{CA} (Å)	V_p (Å^3)	ρ (e$^-$ Å^{-3})	$R_{CA} - R_1$ (Å)	Ξ
Cs	1	1.67	0.60	28.53	60.67	1.01×10^6	0.181	32	272
K	1	1.33	0.75	25.87	54.13	9.38×10^5	0.104	28	253
Na	1	0.98	1.02	21.24	43.53	6.55×10^5	0.099	22	176
Li	1	0.68	1.47	22.13	44.01	6.44×10^5	0.079	22	174
Ba	2	1.34	1.49	17.88	41.59	6.93×10^5	0.101	24	187
Zn	2	0.74	2.70	20.79	42.96	7.96×10^5	0.124	22	214
Mg	2	0.65	3.08	20.02	41.17	8.42×10^5	0.095	21	227

radius. No further attempt will be made to explain this disagreement, but these effects may be important for the mechanical properties of these materials.[19]

Conclusions

In this paper, the morphology of MAn-*g*-EPM based ionomers was measured by SAXS and interpreted with the help of the Yarusso−Cooper model. The modified hard-sphere model of Yarusso and Cooper gave a very good fit to the experimental data and accurately describes the morphology of the ionomers and ionomer precursors based on MAn-*g*-EPM. Solid-state NMR results on MAn-*g*-EPM-based ionomers showed the presence of the restricted mobility layer.[20]

The ionomer precursors showed a peak in the SAXS profile similar to the ionomers. The results from a range of precursor materials suggest that there is a critical concentration (DG of approximately 3 wt %) above which aggregation of the polar groups in the apolar matrix occurs.

It was also remarkable that the size of the aggregates of the MAn-*g*-EPM-based systems is much larger than for other reported ionomer systems. As a consequence, the number of acid groups inside an aggregate is much larger compared to systems like Surlyn or sulfonated polystyrene-based ionomers. Therefore, it is not surprising that the aggregates contain a substantial amount of EPM chain fragments. Depending on degree of neutralization, the volume fraction of MAn inside an aggregate is at least 40 vol %; this is taken into account in the proposed model of the aggregates (Figure 5). The presence of a large amount of EPM in the aggregates has a pronounced effect on the mechanical properties.[19] The presence of ionic aggregates greatly affects the properties of the ionomers. The study of mechanical properties and melt processability revealed that the MAn-*g*-EPM-based ionomers exhibit good mechanical properties and acceptable melt viscosities. One of the most pronounced effects of neutralization was the increase in melt viscosity. Furthermore, an increasing DN and/or DG resulted in increasing tensile strength, hardness, and gel content, but a decreasing elongation at break and compression set.

In the case of ionomers neutralized by divalent cations, it was observed that the morphology changes drastically when the degree of neutralization exceeds 50%. The number of aggregates decreases and the size of the aggregates increases at DN = 50%. Before and after DN = 50% the changes are not as remarkable as this change. The ionic aggregate size depends on the valency of neutralizing cation used for neutralization. The alkali metal cations showed on increasing ionic radius an increasing ionic aggregate radius, radius of closest approach, and increasing thickness of the restricted mobility layer. However, the alkaline earth metal cation series showed a decreasing ionic radius upon increasing cation radius. This behavior can be related to the coordination of the cations with the carboxylic acid groups of the grafted MAn units.

Further, the results of a series of ionomers based on MAn-*g*-EPM with a DG of 7.33 wt % showed a tightening of the aggregates upon increasing DN, and with solid-state NMR a reduced mobility upon increasing DN was observed. This suggests that the strength of aggregates increases upon increasing degree of neutralization. Overall, it was observed that upon neutralization the average dimension of the core of the scattering particle (R_1) remains about the same, but the restricted mobility layer (R_{CA}) increases more substantially.

Acknowledgment. The authors thank DSM Research for financial support. We also thank Prof. T. Michels (Eindhoven University of Technology) for helpful discussions on the modeling of the SAXS results. Dr. Günther Grossmann of the CLRC Daresbury Laboratory is acknowledged for his assistance during the SAXS measurements. The silver behenate was a kind gift of Dr. Tom Blanton from Kodak.

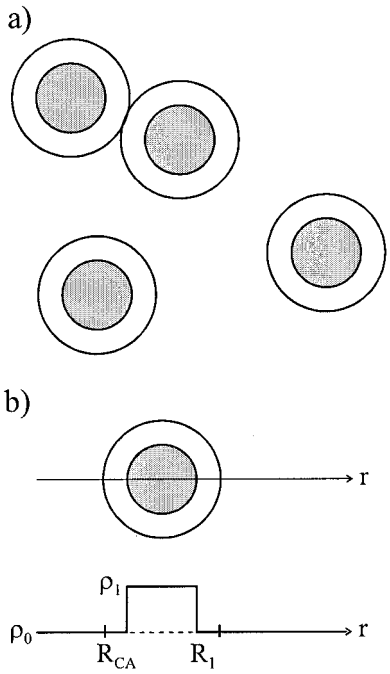

Figure 7. (a) Modified hard-sphere model. (b) Corresponding electron density profile.

Table 4. Statistics of the Nonlinear Least-Squares Fitting Procedure for a Zinc Ionomer Based on MAn-*g*-EPM (DG = 7.33 wt %, DN = 20%)

	estimate	asymptotic std error	asymptotic 95% confidence interval	
			lower	upper
R_1	22.19	0.13	21.93	22.45
R_{CA}	44.79	0.09	44.61	44.97
V_p	5.93×10^5	5.94×10^3	5.81×10^5	6.05×10^5
ρ	0.100	0.001	0.098	0.102

Table 5. Parameter Correlation Matrix

	R_1	R_{CA}	V_p	ρ
R_1	1	−0.44	−0.05	−0.89
R_{CA}	−0.44	1	0.28	0.42
V_p	−0.05	0.28	1	0.46
ρ	−0.89	0.42	0.46	1

Appendix A. The Fitting Procedure

The Yarusso and Cooper model provided the best fit for the MAn-*g*-EPM-based ionomers. In this model, the ionic aggregates are considered as spherical particles with a high electron dense ionic core with radius R_1 and a shell of hydrocarbons with restricted mobility with radius R_{CA} arranged with a liquidlike degree of order with a closest approach distance between two aggregates of $2R_{CA}$. The average sample volume per aggregate is defined as V_p. The electron density difference between the core and the shell, which has the same electron density as the matrix, is defined as ρ. The model, depicted in Figure 7 and given by eq A, has four adaptable fit parameters, i.e., R_1, R_{CA}, V_p, and ρ. Model calculations showed that in the Yarusso−Cooper model the parameter R_{CA} determines mainly the peak position and the peak width. When R_{CA} is increased and all other parameters are kept constant, the position of the peak shifts to lower values of q and the peak becomes sharper. The other parameters, i.e., R_1, V_p, and ρ, hardly affect the position of the peak. When the value of R_1 is increased, the intensity of the peak increases, and the peak broadens to some extent. On increasing V_p, the intensity of the peak decreases, which can be explained by the decreasing number of particles in the sample. An increasing scattering contrast between the matrix and the ionic aggregates (ρ) causes an increase in intensity.

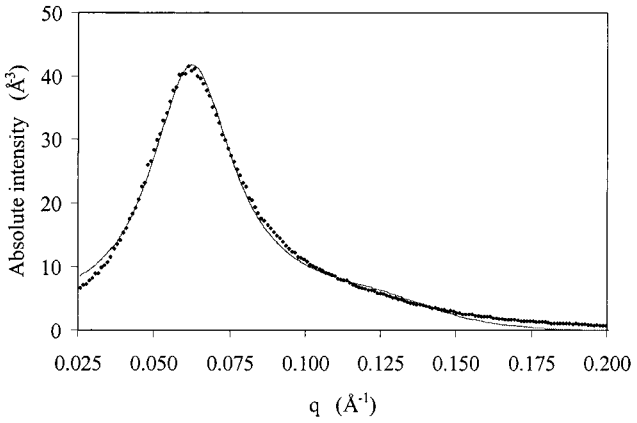

Figure 8. Fit of the Yarusso and Cooper model to the experimental data for a zinc ionomer based on MAn-*g*-EPM with DG = 7.33 wt % and DN = 20%, where the diamonds denote the experimental data, and the solid line was calculated using the following parameters: $R_1 = 22.2$ Å, $R_{CA} = 44.8$ Å, $V_p = 5.93 \times 10^5$ Å^3, and $\rho = 0.100$ e$^-$ Å^{-3}.

In this appendix, the fitting procedure will be discussed in more detail to gain more insight into possible correlations between the parameter and the influence of the individual parameters on the peak profile.

$$\frac{I(q)}{I_e(q)V} = \frac{1}{V_p} V_1^2 \rho^2 \Phi^2(qR_1) \frac{1}{1 + \frac{8V_{CA}}{V_p}\epsilon\Phi(2qR_{CA})} \quad \text{(A.1)}$$

where

$$\Phi(x) = 3\,\frac{\sin x - x\cos x}{x^3} \quad \text{(A.2)}$$

and I_e is the scattered intensity by a single electron under the experimental conditions, V is the scattering volume, ϵ is a constant very close to one, $V_1 = (4\pi/3)R_1^3$, and $V_{CA} = (4\pi/3)R_{CA}^3$.

SAS software (Statistical Analysis System, SAS-Institute Inc., Cary, North Carolina) was used to fit the model to the experimental data. A representative example of the comparison of the experimental data and the best fit is shown in Figure 8. The best-fit values of the four model parameters were found by a nonlinear least-squares fitting procedure. The Newton−Gauss method was used because of its numerical stability and fast convergence. An estimation of the best-fit parameter value set is obtained as well as the number of iterations necessary for convergence. In addition, the uncertainty of each best-fit parameter value is given by a 95% confidence interval (Table 4).

Besides the best-fit parameter set, the correlation matrix (Table 5) is given, from which information can be obtained about the degree of correlation between the parameters. If the parameters are strongly correlated (correlation coefficient is larger than 0.98), problems

may arise in finding a unique set of parameters. As can be seen in the parameter correlation matrix, all four parameters are more or less independent for the materials studied and independent of the sample-to-detector distances.[30] Therefore, the fitting procedure results in a unique set of best-fit values.

References and Notes

(1) *Ionic Polymers*; Holliday, L., Ed.; Applied Science Publishers: London, 1975.
(2) *Ions in Polymers*; Eisenberg, A., Ed.; Advances in Chemistry; American Chemical Society: Washington, DC, 1980; p 187.
(3) *Ionomers: Characterizations, Theory, and Applications*; Schlick, S., Ed.; CRC Press Inc.: Boca Raton, FL, 1996.
(4) *Ionomers: Synthesis, Structure, Properties and Applications*; Tant, M. R., Mauritz, K. A., Wilkes, G. L., Eds.; Chapman & Hall: London, 1997.
(5) Kutsumizu, S.; Tagawa, H.; Muroga, Y.; Yano, S. *Macromolecules* **2000**, *33*, 3818.
(6) Agarwal, P. K.; Lundberg, R. D. *Macromolecules* **1984**, *17*, 1918.
(7) MacKnight, W. J.; Lundberg, R. D. *Rubber Chem. Technol.* **1984**, *57*, 652.
(8) Paeglis, A. U.; O'Shea, F. X. *Rubber Chem. Technol.* **1988**, *61*, 223.
(9) Oostenbrink, A. J.; Gaymans, R. J. *Polymer* **1992**, *33*, 3086.
(10) Makowski, H. S.; Lundberg, R. D.; Westerman, L.; Bock, J. *Polym. Prepr.* **1978**, *19*, 292.
(11) Lundberg, R. D.; Makowski, H. S.; Westerman, L. In *Ions in Polymers*; Eisenberg, A., Ed.; Advances in Chemistry Series 187; American Chemical Society: Washington, DC, 1980; Chapter 5.
(12) Lundberg, R. D.; Makowski, H. S. In *Ions in Polymers*; Eisenberg, A., Ed.; American Chemical Society: Washington, DC, 1980; Chapter 2.
(13) Marx, C.; Claufield, D.; Cooper, S. L. *Macromolecules* **1973**, *6*, 344.
(14) Yarusso, D. J.; Cooper, S. L. *Macromolecules* **1983**, *16*, 1871.
(15) Guinier, A.; Fournet, G. *Small Angle Scattering of X-rays*; Wiley: New York, 1955.
(16) Debye, P. *Phys. Z.* **1927**, *28*, 13.
(17) Eisenberg, A.; Hird, B.; Moore, R. B. *Macromolecules* **1990**, *23*, 4098.
(18) MacKnight, W. J.; Taggert, W.; Stein, R. *J. Polym. Sci., Symp.* **1974**, *45*, 113.
(19) Wouters, M. E. L. Ph.D. Thesis, Eindhoven University of Technology, 2000.
(20) Wouters, M. E. L.; et al., to be published.
(21) Bras, W.; Derbyshire, G. E.; Ryan, A. J.; Mant, G. R.; Felton, A.; Lewis, R. A.; Hall, C. J.; Greaves, G. N. *Nucl. Instrum. Methods Phys. Res.* **1993**, *A326*, 587.
(22) Huang, T. C.; Toraya, H.; Blanton, T. N.; Wu, Y. *J. Appl. Crystallogr.* **1993**, *26*, 180.
(23) Russell, T. P.; Lin, J. S.; Spooner, S.; Wignall, G. D. *J. Appl. Crystallogr.* **1988**, *21*, 629.
(24) Eisenberg, A.; Navratil, M. *Macromolecules* **1974**, *7*, 90.
(25) Roche, E. J.; Stein, R. S.; MacKnight, W. J. *J. Polym. Sci., Polym. Phys. Ed.* **1980**, *18*, 1035.
(26) Peiffer, D. G.; Weiss, R. A.; Lundberg, R. D. *J. Polym. Sci., Polym. Phys. Ed.* **1982**, *20*, 1503.
(27) The miscibility of MAn and EPM is a particular example of a result of the large polarity difference. Studies on the grafting of MAn in the polymer melt have shown that the limited solubility of MAn in the apolar polymer melt results in low grafting efficiencies. Because of the poor solubility and the polar character of the MAn, it is reasonable to assume that the grafted MAn units form a separate phase in the apolar EPM matrix.
(28) Wouters, M. E. L.; et al., to be published.
(29) Hogt, A. H. *Compalloy '90* **1990**, 179.
(30) Different sample-to-detector distances were used for some samples studied. These distances were 1.5, 3.5, and 7 m. All three experimental setups resulted in the same scattering profile. The parent EPM did not show any peak in the SAXS profile. The profiles of the MAn-*g*-EPM materials all showed only one peak at a q value of about 0.06 $Å^{-1}$.

MA0107253